Kovove Mater. 49 2011 75–83
DOI: 10.4149/km_2011_1_75

Creep behavior of metals processed by equal-channel angular pressing

M. Kawasaki[1]*, V. Sklenička[2], T. G. Langdon[1,3]

[1] *Departments of Aerospace & Mechanical Engineering and Materials Science, University of Southern California, Los Angeles, CA 90089-1453, U.S.A.*
[2] *Institute of Physics of Materials, Academy of Sciences of the Czech Republic, Žižkova 22, CZ-616 62 Brno, Czech Republic*
[3] *Materials Research Group, School of Engineering Sciences, University of Southampton, Southampton SO17 1BJ, U.K.*

Received 22 June 2010, received in revised form 10 August 2010, accepted 20 August 2010

Abstract

The processing of metals by equal-channel angular pressing provides the capability of refining the grain size to the submicrometer or nanometer level. It is shown that this will influence the high temperature creep properties provided the ultrafine grains are reasonably stable at elevated temperatures. Examples are presented for high-purity aluminum where grain growth occurs easily and some aluminum-based alloys where grain growth is restricted through the presence of scandium additions. It is relatively easy to depict the creep behavior by plotting deformation mechanism maps. Two examples of these maps are presented for the Pb-62%Sn eutectic alloy and high-purity aluminum.

K e y w o r d s: creep, deformation mechanism maps, equal-channel angular pressing, flow mechanisms, grain boundary sliding

1. Introduction

The mechanical properties of crystalline materials divide into two broad regimes depending upon the testing temperature. In the low temperature region the deformation mechanisms depend upon thermally-activated processes whereas at high temperatures the flow behavior depends upon diffusion-controlled processes. The flow behavior in the high temperature regime is designated creep when tests are conducted under conditions of constant load or constant stress and the creep process becomes important typically at temperatures above $\sim 0.5\,T_{\mathrm{m}}$, where T_{m} is the absolute melting temperature of the material.

A material tested under creep conditions generally exhibits three distinct regions of flow. The primary region refers to the initial stage of creep where the creep rate is decreasing, the secondary or steady-state stage refers to a region in which the creep rate remains constant and the tertiary stage is a region where the creep rate accelerates to final fracture. The steady-state stage is often the dominant region in many practical situations and therefore much attention has been devoted to interpreting and identifying the various deformation mechanisms occurring within this region.

Although creep is an exceptionally old area of research, dating back to the classic work of Phillips [1] over one-hundred years ago, new processing techniques have become available over the last two decades which provide an opportunity to expand the creep behavior into new areas that were not feasible in earlier experiments. These new opportunities arise because of the potential for achieving remarkable grain refinement in bulk metals through the application of severe plastic deformation (SPD) [2]. To place this report in perspective, the next section briefly reviews the principles of creep and it shows where SPD processing may be used to make new contributions in high temperature deformation and the following section describes representative results that are now available describing the use of this new approach.

*Corresponding author: tel.: +1-213-740-4342; fax +1-213-740-8071; e-mail address: mkawasak@usc.edu

2. Principles of creep

Experimental measurements taken in the laboratory generally show that the steady-state creep rate, $\dot{\varepsilon}$, varies with the applied stress, σ, through a power-law relationship of the form

$$\dot{\varepsilon} = A_1 \sigma^n, \tag{1}$$

where A_1 is a constant and n is the stress exponent for creep. At exceptionally high applied stresses the creep rate varies exponentially with the applied stress so that Eq. (1) becomes

$$\dot{\varepsilon} = A_2 \exp(B\sigma), \tag{2}$$

where A_2 and B are appropriate constants. The point of transition from power-law creep and Eq. (1) at lower stresses to an exponential form of creep and Eq. (2) at high stresses is generally termed power-law breakdown (PLB).

Equation (1) is a simple relationship describing the steady-state strain rate in terms of the applied stress but in practice the measured creep rates depend upon the precise testing conditions including the testing temperature and the grain size of the material. This means it is possible to express Eq. (1) in a more explicit form given by

$$\dot{\varepsilon} = \frac{ADGb}{kT} \left(\frac{b}{d}\right)^p \left(\frac{\sigma}{G}\right)^n, \tag{3}$$

where A is a dimensionless constant, D is the diffusion coefficient, G is the shear modulus of the material, b is the Burgers vector, k is Boltzmann's constant, T is the absolute temperature, d is the grain size and p is the exponent of the inverse grain size. The diffusion coefficient is given by $D_o \exp(-Q/RT)$, where D_o is a frequency factor, Q is the activation energy for the rate-controlling diffusive process and R is the gas constant. It follows from inspection of Eq. (3) that the steady-state creep rate is defined exclusively by the values of only four terms: A, Q, p and n.

All creep mechanisms follow a relationship of the form given in Eq. (3) and Fig. 1 shows the type of behavior that is observed if the steady-state creep rate is plotted logarithmically against the applied stress. Over a wide range of intermediate stresses, creep occurs through the intragranular movement of dislocations and the strain rate is then independent of the grain size so that $p = 0$ in Eq. (3): this region is labeled dislocation creep in Fig. 1. At very high stresses there is a transition to flow by Eq. (2) in the region of PLB and at low stresses the stress exponent is reduced to a value of 1 or 2 and there is a transition in the rate-controlling process to mechanisms such as diffusion creep, Harper-Dorn creep or grain boundary sliding.

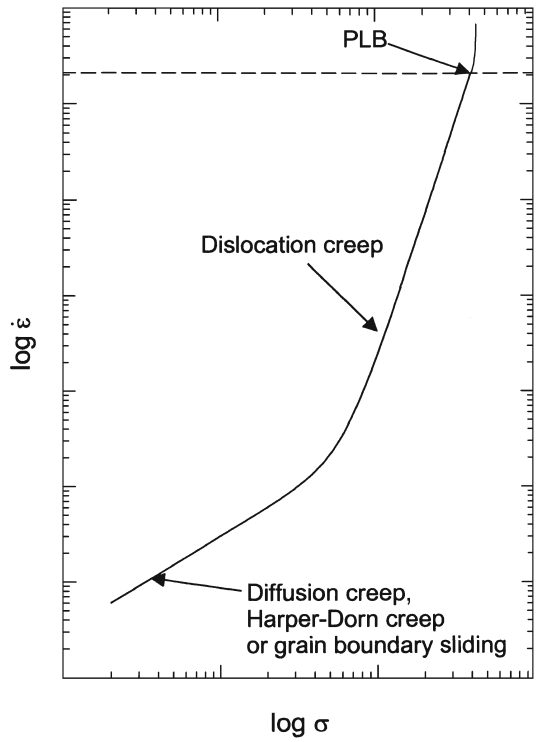

Fig. 1. Schematic illustration of the typical variation of the steady-state strain rate with stress in the regime of high temperature creep.

This low stress region may have a dependence on grain size because there are values of p of 2 or 3 for Nabarro-Herring diffusion creep [3, 4] and Coble diffusion creep [5], respectively, whereas in Harper-Dorn creep [6, 7] there is no dependence on grain size so that $p = 0$ and in grain boundary sliding in superplastic flow there is a value of $p = 2$ [8].

Figure 1 demonstrates the importance of small grain sizes in delineating the creep behavior at very low stresses. Traditionally, small grain sizes are achieved in metallic alloys through appropriate thermo-mechanical processing but this leads to a minimum grain size that is typically in the range of ~ 2–5 μm. Much smaller grain sizes, in the submicrometer or even the nanometer range, may be achieved by using SPD processing in techniques such as equal-channel angular pressing (ECAP) [9] or high-pressure torsion (HPT) [10]. In ECAP a sample, in the form of a rod or bar, is inserted into a channel in a special die and it is then pressed through the die so that it experiences a very high strain as it passes through an abrupt angle incorporated into the channel. Thereafter, repetitive pressings may be undertaken to impose even higher strains. In HPT the sample, in the form of a relatively thin disk, is placed between massive anvils and subjected to a high applied pressure and concurrent torsional straining. Both of these procedures are

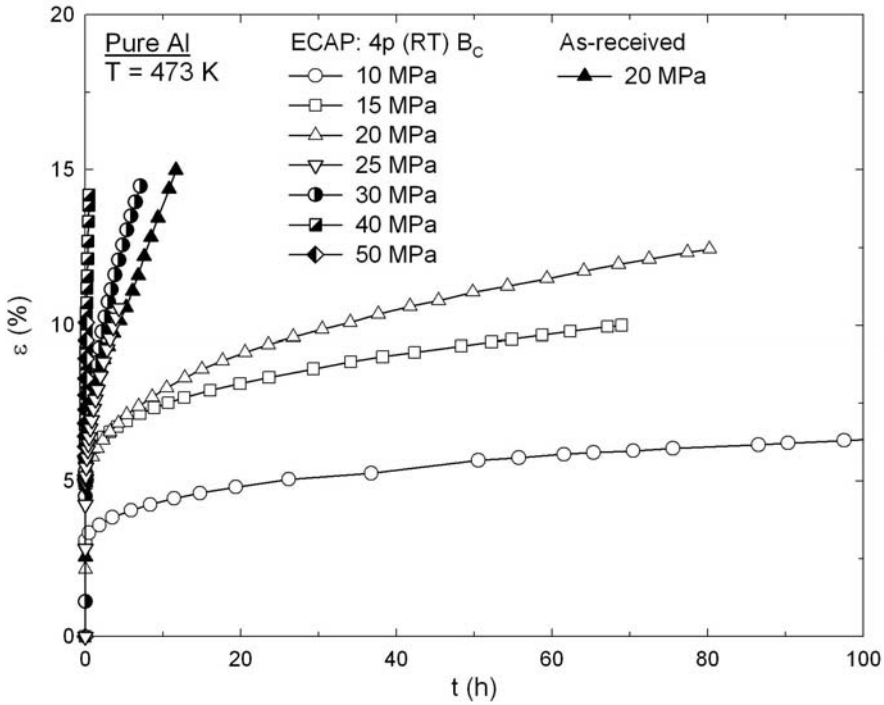

Fig. 2. Strain versus time for high-purity aluminum tested at 473 K after processing by ECAP [14]: a creep curve for an unprocessed sample is also shown.

effective in introducing very significant grain refinement although generally it is possible to achieve smaller grains when using HPT.

The ability to produce materials with exceptionally small grains means that flow processes such as diffusion creep and grain boundary sliding may become more important in the creep of these materials because these mechanisms have $p \neq 0$. However, in order to take advantage of this capability, it is necessary that these ultrafine grains are reasonably stable at elevated temperatures so that the grain size remains small during high temperature testing. In practice, there are numerous reports documenting the occurrence of grain growth in ultrafine-grained materials at elevated temperatures [11–13]. Thus, the importance of making use of SPD processing in creep studies will depend critically upon the thermal stability of the processed metals.

3. Examples of the creep of materials processed using ECAP

3.1. Creep behavior of high-purity aluminum

An earlier report described the creep properties of high-purity (99.99 %) aluminum processed by ECAP at room temperature [14]. In this investigation, the initial grain size in the annealed condition was $\sim$ 1 mm and this was reduced to $\sim$ 1.3 μm by pressing for 4 passes at room temperature using an ECAP die containing a channel bent through an angle of 90° and with an outer arc of curvature of 20° at the point of intersection of the two channels. It can be shown that these angles lead to an imposed strain of $\sim$ 1 on each separate passage through the die [15] and the samples were processed using route B_C in which each billet is rotated by 90° in the same sense about the longitudinal axis between passes [16]. The processing route B_C was used because it led most expeditiously to an array of equiaxed grains separate by boundaries having high angles of misorientation [17].

Figure 2 shows an example of the creep curves obtained for pure Al after processing by ECAP. The curves in Fig. 2 plot the strain, ε, against the time, t, and results are shown for samples tested in tensile creep under conditions of constant stress at a temperature of 473 K using various stresses from 10 to 50 MPa: for comparison, Fig. 2 also includes a curve for an unprocessed sample tested at a stress of 20 MPa. All of the creep curves obtained in these experiments were of the conventional form with an initial short primary stage of creep and a well-defined steady-state region.

Following Eq. (3), it is convenient to logarithmically plot the measured steady-state creep rate against the applied stress since the slope of this plot will give the stress exponent, n. This plot is shown in Fig. 3 for the same samples illustrated in Fig. 2 and the plot includes also the datum point for the aluminum in the as-received condition. It follows from Fig. 3 that the stress exponent for the samples processed by ECAP

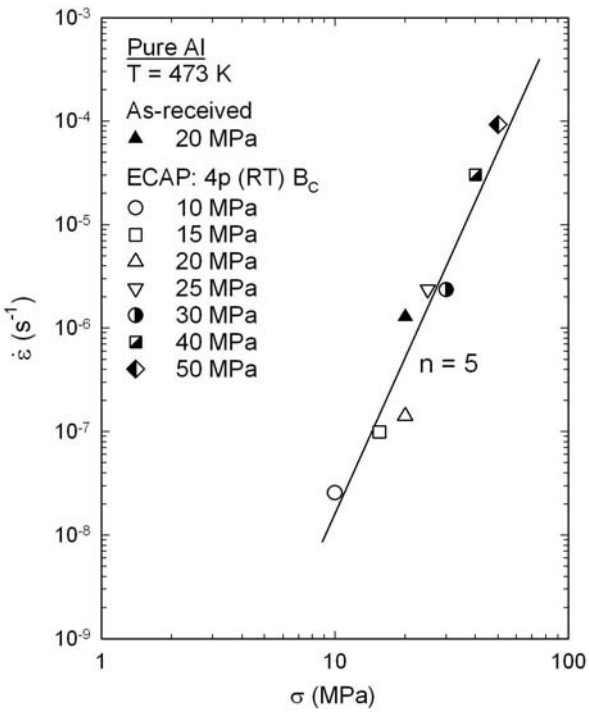

Fig. 3. Steady-state creep rate versus stress at 473 K for high-purity Al processed by ECAP and for an unprocessed sample [14].

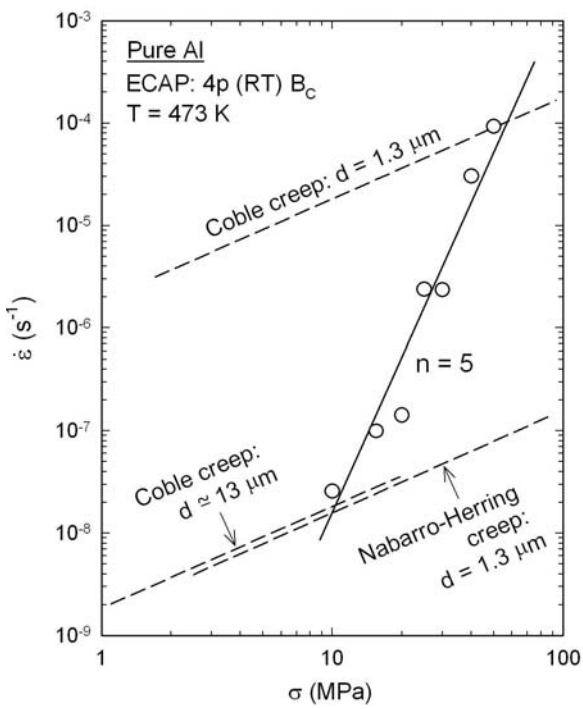

Fig. 4. The experimental datum points for the samples processed by ECAP in Fig. 3 together with predictions for Nabarro–Herring and Coble diffusion creep for different grain sizes [19].

is $n \approx 5$ where this value suggests an intragranular dislocation creep mechanism rather than a flow process dependent upon the presence of grain boundaries. This value for n is consistent also with earlier values of ~ 4.8 and ~ 5.7 reported for pure aluminum after processing by ECAP and creep testing in compression and tension, respectively [18]. It is also apparent from Fig. 3 that the experimental datum point for the unprocessed sample lies very close to the line for the samples processed by ECAP.

In order to understand this result, it is necessary to look in more detail at the possible deformation mechanisms. Taking the grain size after ECAP as $d \approx 1.3\,\mu m$, Fig. 4 shows, on a logarithmic plot of strain rate against stress, the behavior predicted for Nabarro-Herring [3, 4] and Coble [5] diffusion creep where $n = 1$ and the values of p are either 2 or 3, respectively [19]. The lower line for Nabarro-Herring creep demonstrates that this process is too slow to have any significant influence on the creep behavior of the pure aluminum. By contrast, the upper line for Coble diffusion creep with $d = 1.3\,\mu m$ suggests that this mechanism should play a critical role in the creep properties.

The reason that diffusion creep is not experienced in the pure aluminum processed by ECAP is because the pure metal contains no precipitates and therefore the ultrafine grains are not stable when testing at elevated temperatures. It was shown in annealing experiments at 473 K, the same temperature used in the creep testing, that the grains grow by about one order of magnitude prior to, or in the very early stages of, the creep deformation. Because of this grain growth, the grain size during creep testing is probably about one order of magnitude larger than measured immediately after ECAP processing. Accordingly, taking a grain size for the creep experiments of $d \approx 13\,\mu m$, the lower line for Coble creep in Fig. 4 shows the predicted behavior for these conditions. This line is below the lowest experimental datum point.

The important conclusion from these experiments on high-purity aluminum is that the ultrafine grains produced by ECAP are unstable at high temperatures and therefore the measured creep behavior in this pure metal is similar to that recorded in conventional high-purity aluminum without processing by ECAP.

3.2. Creep behavior of aluminum alloys containing precipitates to restrict grain growth

The preceding section demonstrates that ECAP processing will be effective for achieving new creep properties only in materials containing precipitates that are capable of preventing, or at least hindering, the growth of the ultrafine grains at high temperatures. The Al-3%Mg-0.2%Sc alloy is an example of an

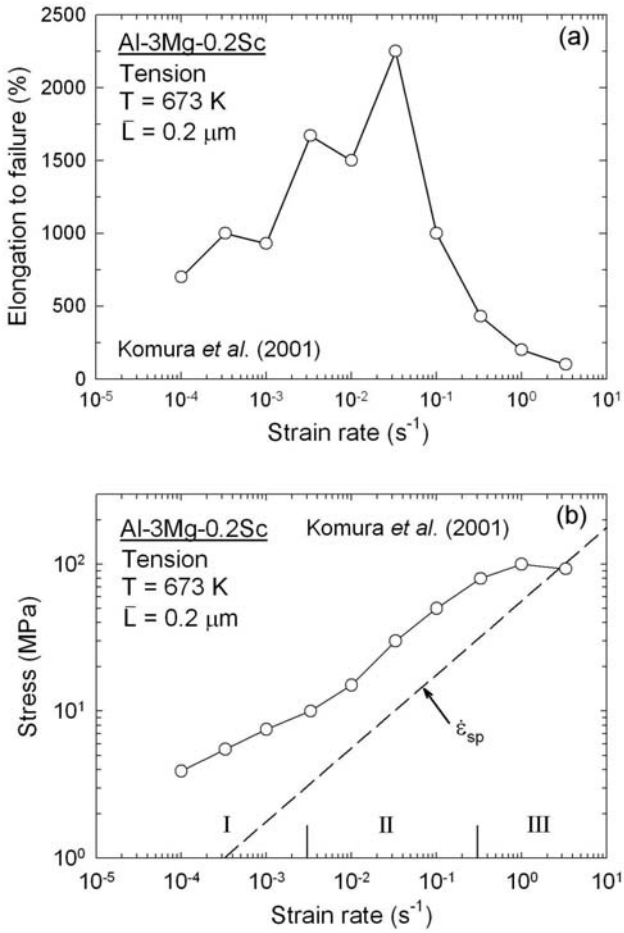

Fig. 5. Results for the Al-3%Mg-0.2% Sc alloy showing (a) the elongations to failure as a function of strain rate at 673 K and (b) the variation of flow stress with strain rate [22]: the lower broken line denotes the theoretical prediction for superplastic flow [29].

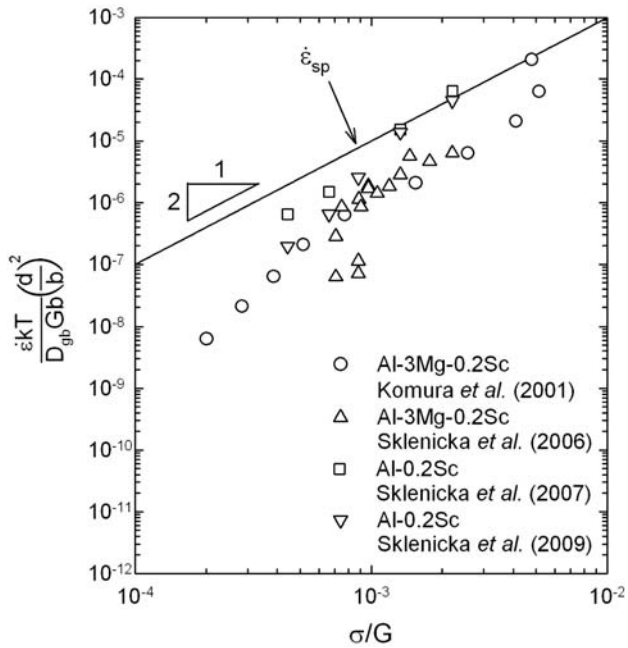

Fig. 6. Temperature and grain size compensated creep rate versus normalized stress for aluminum alloys containing scandium [22, 30–32]: the upper line is the theoretical prediction for superplastic flow [29].

alloy where the presence of scandium is effective in severely restricting grain growth up to temperatures of at least 800 K [20] and thereby giving a capability for achieving excellent superplastic ductilities at elevated temperatures [21–23].

An Al-3%Mg-0.2%Sc alloy was processed by ECAP at room temperature for 8 passes using a die with an internal angle of 90° and this gave a mean linear intercept grain size, $\bar{L}$, of 0.2 μm where the spatial grain size, d, is equal to $1.74 \times \bar{L}$ [24]. Figure 5a shows the measured elongations to failure for samples processed by ECAP and then pulled to failure in tension at different strain rates using a testing temperature of 673 K [22]. These results are unusual because some of the elongations are exceptionally high and, in addition, they occur at very rapid strain rates: the occurrence of very high elongations at strain rates $\geq 10^{-2}\,\mathrm{s}^{-1}$ shows that this behavior is within the regime designated as high strain rate superplasticity [25].

When the measured flow stresses for each sample are plotted logarithmically against the imposed strain rate, the result is shown in Fig. 5b where the datum points now lie along a sigmoidal curve which is characteristic of conventional superplastic alloys in which the optimum superplastic ductilities occur at intermediate strain rates in region II and the ductilities decrease at both slower strain rates in region I and faster strain rates in region III [26, 27]. When materials deform superplastically, it is now well established that the rate-controlling process is grain boundary sliding [28]. Therefore, it is valuable to compare the measured strain rates within the superplastic region with the theoretical strain rate for superplastic flow controlled by grain boundary sliding, $\dot{\varepsilon}_{\mathrm{sp}}$ [8]. This comparison is shown in Fig. 5b where the broken line delineates the theoretical prediction and it is apparent that this prediction is in good agreement, to within an order of magnitude, with the experimental data at strain rates where the elongations to failure are > 1000 % [29]. This agreement confirms that the conventional relationship for superplastic flow applies equally to materials processed by ECAP where the grain sizes are within the submicrometer range.

An alternative approach is shown in Fig. 6 where data for the Al-3%Mg-0.2%Sc alloy [22] are plotted logarithmically in the form of the temperature and grain size compensated strain rate, $(\dot{\varepsilon}kT/D_{\mathrm{gb}}Gb) \cdot (d/b)^2$, against the normalized stress, σ/G, where $D = D_{\mathrm{gb}}$ for grain boundary diffusion and $p = 2$ are contained within the fundamental relationship for su-

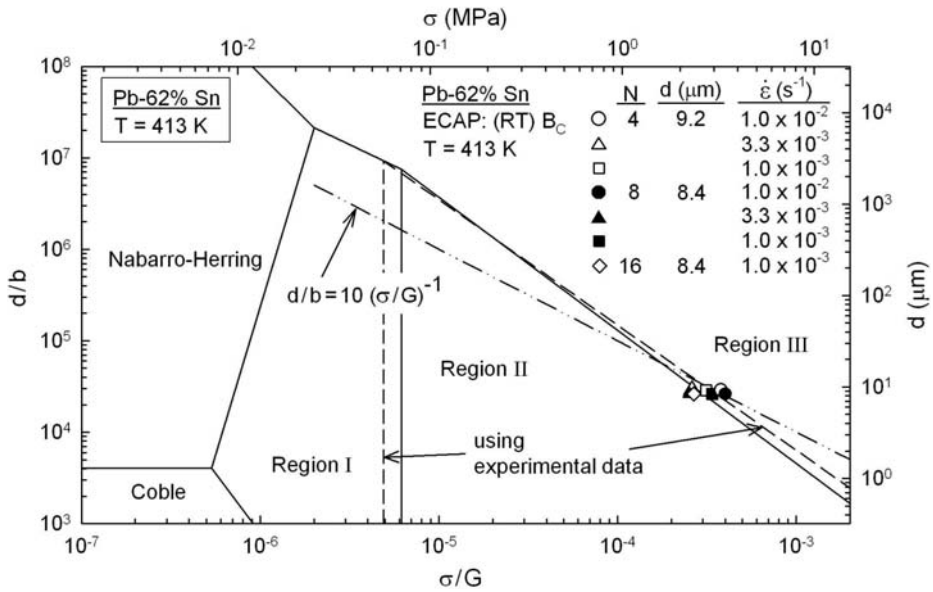

Fig. 7. Deformation mechanism map for a Pb-62%Sn alloy at a temperature of 413 K [41].

perplastic flow [8]. This plot also includes other data for an Al-3%Mg-0.2%Sc alloy processed by ECAP [30] and an Al-0.2%Sc alloy processed by ECAP and tested in compression [31] or tension [32]: all processing of these materials by ECAP was conducted at room temperature through 8 passes using a die with an angle of 90°, the mean linear intercept grain sizes for the three alloys were 1.5, 0.9 and 0.55 μm, respectively, and all of the subsequent testing was conducted at a temperature of 473 K. The upper solid line in Fig. 6 shows the theoretical relationship for $\dot{\varepsilon}_{sp}$ and again there is very good agreement, to within one order of magnitude, for almost all of the datum points for all four materials [29].

The agreement between the experimental data and the theoretical model is encouraging because it means that standard creep relationships may be used in interpreting materials processed by ECAP. Furthermore, there are now a number of reports of superplastic behavior in materials processed to produce ultrafine grain sizes by ECAP [33] and the present results confirm the potential for using ECAP to expand the field of superplasticity into new areas [34]. An example of the remarkable potential provided by ECAP processing is the recent report of a record superplastic elongation of 3050 % achieved in a magnesium ZK60 alloy after processing through 2 passes by ECAP [35].

3.3. Representation of creep data on deformation mechanism maps

The concept of plotting deformation mechanism maps goes back to a very early report where all possible deformation mechanisms were plotted on a single diagram having coordinates of the logarithmic normalized stress, σ/G, against the homologous temperature, T/T_m, at constant grain size [36]. In this representation, the map covers all temperatures from absolute zero to the melting temperature and it is divided into separate fields within which a specified mechanism is dominant. It is also feasible to superimpose strain rate contours onto the map to indicate both the flow mechanism and the relevant strain rate under any selected testing conditions [37]. However, in this early format it was difficult to construct the maps because the field boundaries and the strain rate contours appear as curved lines. Subsequently, the maps were developed in a simpler and easy-to-construct format for high temperature creep by plotting in three different formats: σ/G against T_m/T at constant grain size [38], normalized grain size, d/b, against σ/G at constant temperature [39] and d/b against T_m/T at constant stress [40].

Typically, the early maps were constructed using grain sizes of 100 μm or larger but the production of materials with ultrafine grain sizes provides the opportunity to produce deformation mechanism maps for materials having much smaller grain sizes. Figure 7 shows the first deformation mechanism map constructed for an ultrafine-grained material processed by ECAP [41]. This map was prepared for the Pb-62%Sn eutectic alloy processed by ECAP at room temperature and then tested in tension at a temperature of 413 K. The map plots normalized grain size against normalized stress where the individual values of grain size and stress are given on the right-hand and upper axes, respectively. The map is divided into separate fields for Nabarro-Herring and Coble diffusion creep and the three basic regions of superplastic flow designated regions I, II and III where region II repres-

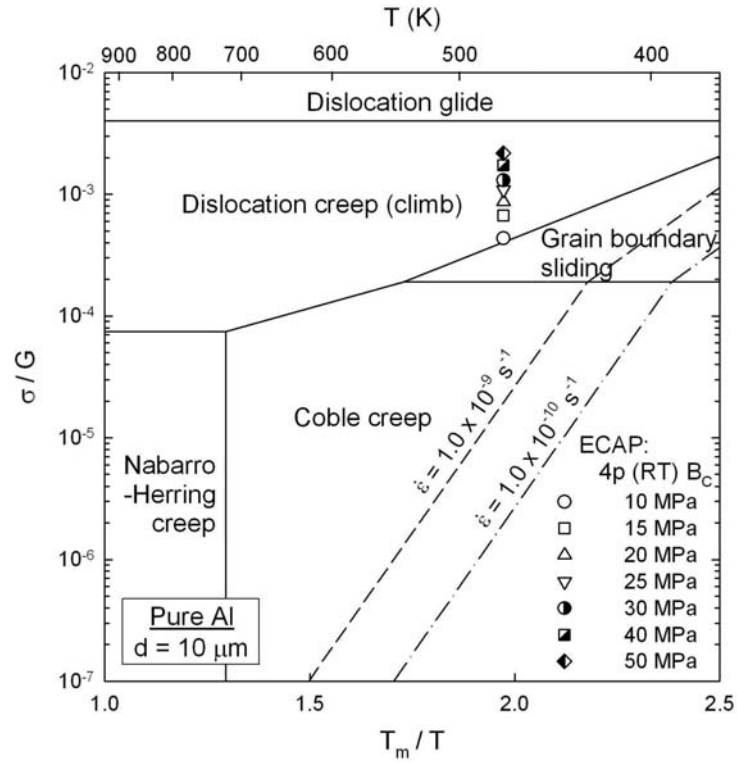

Fig. 8. Deformation mechanism map for high-purity aluminum with a grain size of 10 μm [44].

ents the superplastic behavior. The solid lines delineating the field boundaries were calculated using theoretical relationships including the equation for grain boundary sliding in superplasticity [8] which was used successfully to describe the experimental data for the aluminum alloys in Fig. 6: the dashed field boundaries on the map are based on equations derived from an early investigation of the creep properties of the Pb-62%Sn alloy [42]. Finally, the broken line for $d/b = 10(\sigma/G)^{-1}$ corresponds to the condition where the grain size is equal to the subgrain size in high temperature creep and, as anticipated, this line lies very close to the boundary separating regions II and III [43].

It is apparent from inspection of Fig. 7 that both the theoretical map and the experimental map are similar, thereby again confirming the validity of the theoretical relationships. The experimental points shown in Fig. 7 are based on data obtained from the tensile testing of the Pb-62%Sn alloy after ECAP processing where N gives the number of passes in ECAP when using a die with a channel angle of 90° [41]. This alloy exhibited excellent superplastic properties after ECAP including a maximum elongation of ∼3060 % when testing at 413 K at an imposed strain rate of $1.0 \times 10^{-3}\,s^{-1}$ after ECAP through 16 passes. It is apparent that the experimental points straddle the boundary between regions II and III and therefore this is consistent with the measured elongations to failure.

An alternative form of map is shown in Fig. 8 where σ/G is plotted against T_m/T for pure Al having a grain size of 10 μm [44]. Superimposed are the experimental points taken from the creep data for high-purity Al described earlier in Figs. 2–4. As anticipated from the earlier calculations, these points lie in the region of intragranular dislocation climb but they extend, at the lowest value of normalized stress, to the field boundary with grain boundary sliding. The map also includes two contours of constant strain rate for 10^{-9} and $10^{-10}\,s^{-1}$. Since contours varying by an order of magnitude will be equally spaced on this map, it suggests that the experimental strain rate for the datum point at the lowest stress will be slightly faster than $10^{-8}\,s^{-1}$. This prediction is consistent with the lowest experimental point in Fig. 3. Finally, it should be noted that the transition in Fig. 8 to dislocation glide at the highest stresses corresponds to the transition to a thermally activated process.

4. Discussion

Processing using SPD procedures such as ECAP and HPT provide an opportunity for producing exceptional grain refinement with grain sizes typically lying in the submicrometer range. These small grain sizes open up the possibility of achieving different flow mechanisms when testing under creep conditions at elevated temperatures. However, these different mechanisms will be realized only if the ultrafine grain sizes

produced by SPD processing are reasonably stable at elevated temperatures.

Two examples are described in this report. First, it is shown that the ultrafine grains produced by ECAP in high-purity aluminum are not sufficiently stable when testing in high temperature creep so that the dominant creep process is an intragranular dislocation mechanism as in metals with large grain sizes. Second, scandium additions of 0.2 % to the Al-3%Mg alloy or pure Al are sufficient to retain a small grain size at high temperatures and this leads to creep data where the stress exponent is ~ 2 and flow occurs by grain boundary sliding as in superplastic deformation.

Finally, it is shown by two examples that the construction of deformation mechanism maps provides a simple and effective procedure for predicting both the rate-controlling creep mechanism and the relevant steady-state creep rates under different experimental conditions.

5. Summary and conclusions

1. The processing of metals by equal-channel angular pressing provides an opportunity to achieve very significant grain refinement to the submicrometer or nanometer level. There is a potential for using these materials to obtain new flow processes in high temperature creep provided the ultrafine grains are reasonably stable at elevated temperatures.

2. The flow behavior is represented most easily by plotting deformation mechanism maps that cover the ranges of temperature, stress and grain size of interest in experimental investigations. Examples of these maps are presented for the Pb-62%Sn eutectic alloy and high-purity aluminum.

Acknowledgements

This work was supported by the National Science Foundation of the United States under Grant No. DMR--0855009.

References

[1] PHILLIPS, P.: Proc. Roy. Soc. London, *19*, 1903–1905, p. 491.
[2] VALIEV, R. Z.—ISLAMGALIEV, R. K.—ALEXANDROV, I. V.: Prog. Mater. Sci., *45*, 2003, p. 103. doi:10.1016/S0079-6425(99)00007-9
[3] NABARRO, F. R. N.: In: Reports of a Conference on Strength of Solids. London, U.K., The Physical Society 1948, p. 75.
[4] HERRING, C.: J. Appl. Phys., *21*, 1950, p. 437. doi:10.1063/1.1699681
[5] COBLE, R. L.: J. Appl. Phys., *34*, 1963, p. 1679. doi:10.1063/1.1702656
[6] HARPER, J. G.—DORN, J. E.: Acta Metall., *5*, 1957, p. 654. doi:10.1016/0001-6160(57)90112-8
[7] KUMAR, P.—KASSNER, M. E.—LANGDON, T. G.: J. Mater. Sci., *42*, 2007, p. 408.
[8] LANGDON, T. G.: Acta Metall. Mater., *42*, 1994, p. 2437. doi:10.1016/0956-7151(94)90322-0
[9] VALIEV, R. Z.—LANGDON, T. G.: Prog. Mater. Sci., *51*, 2006, p. 881. doi:10.1016/j.pmatsci.2006.02.003
[10] ZHILYAEV, A. P.—LANGDON, T. G.: Prog. Mater. Sci., *53*, 2008, p. 893. doi:10.1016/j.pmatsci.2008.03.002
[11] WANG, J.—IWAHASHI, Y.—HORITA, Z.—FURUKAWA, M.—NEMOTO, M.—VALIEV, R. Z.—LANGDON, T. G.: Acta Mater., *44*, 1996, p. 2973. doi:10.1016/1359-6454(95)00395-9
[12] FURUKAWA, M.—IWAHASHI, Y.—HORITA, Z.—NEMOTO, M.—TSENEV, N. K.—VALIEV, R. Z.—LANGDON, T. G.: Acta Mater., *4*, 1997, p. 4751. doi:10.1016/S1359-6454(97)00120-1
[13] HASEGAWA, H.—KOMURA, S.—UTSUNOMIYA, A.—HORITA, Z.—FURUKAWA, M.—NEMOTO, M.—LANGDON, T. G.: Mater. Sci. Eng., *A265*, 1999, p. 188. doi:10.1016/S0921-5093(98)01136-8
[14] KAWASAKI, M.—BEYERLEIN, I. J.—VOGEL, S. C.—LANGDON, T. G.: Acta Mater., *56*, 2008, p. 2307. doi:10.1016/j.actamat.2008.01.023
[15] IWAHASHI, Y.—WANG, J.—HORITA, Z.—NEMOTO, M.—LANGDON, T. G.: Scripta Mater., *35*, 1996, p. 143. doi:10.1016/1359-6462(96)00107-8
[16] FURUKAWA, M.—IWAHASHI, Y.—HORITA, Z.—NEMOTO, M.—LANGDON, T. G.: Mater. Sci. Eng., *A257*, 1998, p. 328. doi:10.1016/S0921-5093(98)00750-3
[17] OH-ISHI, K.—HORITA, Z.—FURUKAWA, M.—NEMOTO, M.—LANGDON, T. G.: Metall. Mater. Trans., *29A*, 1998, p. 2011. doi:10.1007/s11661-998-0027-z
[18] SKLENICKA, V.—DVORAK, J.—KRAL, P.—STONAWSKA, Z.—SVOBODA, M.: Mater. Sci. Eng., *A410–411*, 2005, p. 408. doi:10.1016/j.msea.2005.08.099
[19] XU, C.—KAWASAKI, M.—LANGDON, T. G.: Int. J. Mater. Res., *100*, 2009, p. 750.
[20] BERBON, P. B.—KOMURA, S.—UTSUNOMIYA, A.—HORITA, Z.—FURUKAWA, M.—NEMOTO, M.—LANGDON, T. G.: Mater. Trans., *40*, 1999, p. 772.
[21] KOMURA, S.—HORITA, Z.—FURUKAWA, M.—NEMOTO, M.—LANGDON, T. G.: J. Mater. Res., *15*, 2000, p. 2571. doi:10.1557/JMR.2000.0367
[22] KOMURA, S.—HORITA, Z.—FURUKAWA, M.—NEMOTO, M.—LANGDON, T. G.: Metall. Mater. Trans., *32A*, 2001, p. 707. doi:10.1007/s11661-001-1006-9
[23] AKAMATSU, H.—FUJINAMI, T.—HORITA, Z.—LANGDON, T. G.: Scripta Mater., *44*, 2001, p. 759. doi:10.1016/S1359-6462(00)00666-7
[24] MOHAMED, F. A.—LANGDON, T. G.: Acta Metall., *23*, 1975, p. 2339.
[25] HIGASHI, K.—MABUCHI, M.—LANGDON, T. G.: ISIJ Intl., *36*, 1996, p. 1423. doi:10.2355/isijinternational.36.1423

[26] ISHIKAWA, H.—MOHAMED, F. A.—LANGDON, T. G.: Phil. Mag., *32*, 1975, p. 1269. doi:10.1080/14786437508228105
[27] LANGDON, T. G.: Metall. Trans., *13A*, 1982, p. 689.
[28] LANGDON, T. G.: Mater. Sci. Eng., *A174*, 1994, p. 225. doi:10.1016/0921-5093(94)91092-8
[29] KAWASAKI, M.—SKLENIČKA, V.—LANGDON, T. G.: J. Mater. Sci., 45, 2010, p. 271. doi:10.1007/s10853-009-3975-9
[30] SKLENICKA, V.—DVORAK, J.—SVOBODA, M.—KRAL, P.—KVAPILOVA, M.—HORITA, Z.: In: Ultrafine Grained Materials IV. Eds.: Zhu, Y. T., Langdon, T. G., Horita, Z., Zehetbauer, M., Semiatin, S. L., Lowe, T. C. Warrendale, PA, The Minerals, Metals and Materials Society 2006, p. 459.
[31] SKLENICKA, V.—DVORAK, J.—KVAPILOVA, M.—SVOBODA, M.—KRAL, P.—SAXL, I.—HORITA, Z.: Mater. Sci. Forum, *539–543*, 2007, p. 2904.
[32] SKLENIČKA, V.—DVOŘÁK, J.—KRÁL, P.—SVOBODA, M.—SAXL, I.: Int. J. Mater. Res., *100*, 2009, p. 762.
[33] KAWASAKI, M.—LANGDON, T. G.: J. Mater. Sci., *42*, 2007, p. 1782. doi:10.1007/s10853-006-0954-2
[34] LANGDON, T. G.: J. Mater. Sci., *44*, 2009, p. 5998. doi:10.1007/s10853-009-3780-5
[35] FIGUEIREDO, R. B.—LANGDON, T. G.: Adv. Eng. Mater., *10*, 2008, p. 37. doi:10.1002/adem.200700315
[36] ASHBY, M. F.: Acta Metall., *20*, 1972, p. 887. doi:10.1016/0001-6160(72)90082-X
[37] FROST, H. J.—ASHBY, M. F.: Deformation-Mechanism Maps: The Plasticity and Creep of Metals and Ceramics. Oxford, U.K., Pergamon Press 1982.
[38] LANGDON, T. G.—MOHAMED, F. A.: J. Mater. Sci., *13*, 1978, p. 1282. doi:10.1007/BF00544735
[39] MOHAMED, F. A.—LANGDON, T. G.: Metall. Trans., *5*, 1974, p. 2339. doi:10.1007/BF02644014
[40] LANGDON, T. G.—MOHAMED, F. A.: Mater. Sci. Eng., *32*, 1978, p. 103. doi:10.1016/0025-5416(78)90029-0
[41] KAWASAKI, M.—LEE, S.—LANGDON, T. G.: Scripta Mater., *61*, 2009, p. 963. doi:10.1016/j.scriptamat.2009.08.001
[42] MOHAMED, F. A.—LANGDON, T. G.: Phil. Mag., *32*, 1975, p. 697. doi:10.1080/14786437508221614
[43] MOHAMED, F. A.—LANGDON, T. G.: Scripta Mater., *10*, 1976, p. 759.
[44] KAWASAKI, M.—LANGDON, T. G.: Mater. Sci. Forum, *638–642*, 2010, p. 1965. doi:10.4028/www.scientific.net/MSF.638-642.1965